Optical studies of single-crystal $Nd_{2-x}Ce_xCuO_{4-\delta}$

Ji-Guang Zhang, Xiang-Xin Bi, E. McRae,* and P. C. Eklund
Department of Physics and Astronomy, University of Kentucky, Lexington, Kentucky 40506

B. C. Sales and Mark Mostoller
Solid State Division, Oak Ridge National Laboratory, P.O. Box 2008, Oak Ridge, Tennessee 37831-6033
(Received 13 September 1990)

Optical reflectivity spectra of $Nd_2CuO_{4-\delta}$ and $Nd_{1.8}Ce_{0.2}CuO_{4-\delta}$ single crystals for the polarization $\mathbf{E}\perp\mathbf{c}$ have been investigated over an energy range from 0.005 to 6 eV. Four E_u intralayer phonons are observed for $Nd_2CuO_{4-\delta}$ at 121, 301, 347, and 507 cm^{-1}, in good agreement with preliminary shell-model-calculation results. The oscillator strength of a broad mid-ir band is found to depend on both oxygen deficiency and cerium doping. The far-ir optical conductivity is fit to both the recently proposed marginal-Fermi-liquid model (MFL) and the modified Drude-Lorentz model (MDL). A notch in the far-ir conductivity is observed at 24 meV, in good agreement with the MFL model. Values for the plasma frequency obtained are quite low and suggest that very large mass enhancement exists for the free carriers in these materials. A clear downshift of oscillator strength from (1–2.3)-eV charge-transfer excitation to the mid-ir band is also observed.

I. INTRODUCTION

The discovery of high-temperature superconductivity in the *n*-type cuprates $R_{2-x}Ce_xCuO_{4-\delta}$ (R=Nd, Pr, or Sm) by Tokura, Takagi, and Uchida[1] has significant implications for understanding the nature of the pairing mechanism in cuprate superconductors because it casts doubt on proposals which are tied uniquely to hole conduction. In this paper we present an optical study on single-crystal samples of $Nd_{2-x}Ce_xCuO_{4-\delta}$ (x=0,0.2) which show the effect of Ce doping. Our optical reflectance studies were carried out at room temperature over a wide energy range (0.005–6 eV) on the as-grown *c* face ($\mathbf{E}\perp\mathbf{c}$). Similar to observations on the isostructural compounds $La_{2-x}Sr_xCuO_4$ (Ref. 2) and $La_{2-x}Sr_xNiO_4$,[3] we observe the presence of an unusually broad and strong midinfrared (mid-ir) absorption band in the Ce-doped compound with a band maximum at 0.13 eV. A very weak mid-ir band was detected in the spectrum of the as-grown, insulating crystal. We find the band can be "activated" either by annealing in He or by Ce doping. We have also studied the in-plane, infrared-active TO and associated LO-phonon modes in $Nd_2CuO_{4-\delta}$. Results of a preliminary shell-model calculation for the zone-center TO-mode frequencies based on the same force constants as used for La_2CuO_4 (Ref. 4) are found to be in fairly good agreement with the data, suggesting that there are probably no unusual differences between the optical-phonon modes in *n*- and *p*-type cuprates.

$Nd_2CuO_{4-\delta}$ exhibits the tetragonal T'-phase structure. At room temperature the intralayer CuO_4 square in this T' phase is expanded slightly, and the *c* axis shrinks slightly, relative to the dimensions of the tetragonal T phase of La_2CuO_4.[1,5,6] $Nd_{2-x}Ce_xCuO_{4-\delta}$ is superconducting for $x\sim0.14$–0.18 with a maximum transition temperature $T_c\sim24$ K at $x\sim0.14$, and T_c tends to decrease with increasing x.[1,4] Transport[7–10] and magnetic[11,12] properties of $Nd_{2-x}Ce_xCuO_{4-\delta}$ ($0<x<0.2$) have been studied as a function of composition (x) and temperature (T). Previous optical work on the *n*-type Nd cuprates have been carried out on polycrystalline pellets[13,14] and polycrystalline thin films.[15] The large optical anisotropy in the cuprates makes it quite difficult in polycrystalline samples to separate quantitatively the *c*- and *a*-axis contributions to the spectra. Optical studies on pellet samples[11,12] of $Nd_{2-x}Ce_xCuO_{4-\delta}$ have noted the interesting coexistence of superconductivity and the strength of the normal-state, mid-ir absorption band. However, a strong mid-ir band has also been observed recently in $La_{2-x}Sr_xNiO_4$,[3] even though it has not yet been possible to prepare nickelate samples which exhibit a Meissner effect of $\sim1\%$.[16]

II. EXPERIMENTAL DETAILS

Single crystals of both $Nd_2CuO_{4-\delta}$ and $Nd_{1.8}Ce_{0.2}CuO_{4-\delta}$ were grown using a CuO flux from a high-purity mixture of Nd_2O_3, CeO_2, and CuO in a yttrium-stabilized zirconium crucible. The reflectance spectra were obtained from the natural, smooth *a*-*b* faces of the crystals without cutting or polishing. The orientation of the crystals was confirmed by x-ray diffraction, and the cerium concentration was measured by energy dispersive x-ray (EDX) analysis using a ceramic standard.

Two $Nd_{2-x}Ce_xCuO_{4-\delta}$ crystals (see Table I) were studied in detail. Samples $S1$ and $S2$ are actually the same undoped crystal (x=0) before ($S1$) and after ($S2$) a 900 °C annealing in He gas at ~1 atm for 19 h. Sample $S3$ is Ce doped (x=0.2), and not He annealed. The samples were studied optically at room temperature using two spectrometers in which the single surface reflectance R was determined by careful replacement of the sample

TABLE I. $Nd_{2-x}Ce_xCuO_{4-\delta}$ sample parameters.

Sample	x	Area ($a-b$ plane)	Post-crystal-growth treatment
$S1$	0	2×3 mm^2	none
$S2$	0	2×3 mm^2	annealed at 900 °C, 19 h, He flow
$S3$	0.2	1×1 mm^2	none

with a standard mirror at the focus of a $f/4$ beam whose central ray was incident upon the sample face at $<8°$ with respect to its a-b surface normal. First, for the 40–4000-cm^{-1} range, a modified model FTS-80 (Digilab, Inc.) rapid-scan Fourier transform infrared (FTIR) spectrometer was used, employing a Si bolometer (Infrared Laboratories, Inc.) and a pyroelectric detector for the far- and mid-ir regions, respectively. Second, for the 0.3–6-eV range, a home-built spectrometer using a model 88 prism monochromator (Perkin-Elmer, Inc.) was employed. CaF_2 and SiO_2 prisms, various sources, and detectors were used to cover the spectral range.

The a-b plane dimensions of the samples were 2×3 mm^2 for S_1 (S_2) and only $\sim1\times1$ mm^2 for $S3$. The reflectance results obtained for the 1×1 mm^2 sample using the FTIR spectrometer were not reproducible when the sample was overfilled by the optical beam or by underfilling a mosaic of several such small crystals. We believe that this is due to the spectral inhomogeneity present in the beam leaving the interferometer. That is, the spectral content of the beam is a function of position within the cross section of the beam. Significant modifications to the optics following the interferometer were therefore made so that small crystals with diameters as small as 1 mm could be studied at normal incidence.[17]

III. RESULTS

The a-b plane reflectance data of $Nd_{2-x}Ce_xCuO_{4-\delta}$ crystals for the spectral rangle 0.005–6 eV are shown in Fig. 1. The solid lines in the figure represent the results of model calculations to be discussed below. The spectrum of the as-grown $Nd_2CuO_{4-\delta}$ crystal ($S1$) is shown in the bottom panel of Fig. 1 and is typical of the isostructural and insulating cuprates[4] and nickelates.[3] Consistent with the tetragonal symmetry of this crystal, peaks identified with four ir-active, intralayer phonons are evident below 0.1 eV in the spectrum. The spectrum for post-annealed $Nd_2CuO_{4-\delta}$ ($S2$) is shown in the middle panel. The changes in phonon peak positions due to annealing are quite small (i.e., less than 1%). However, post-annealing in He increases the overall reflectance of the undoped sample by $\sim20\%$ in the lower-energy range. For energy $\omega>1$ eV, the difference between the $S1$ and $S2$ spectra is less than 3%. The top panel in Fig. 1 shows the reflectance of $Nd_{1.8}Ce_{0.2}CuO_{4-\delta}$ ($S3$). The phonon features so evident in the spectrum of undoped samples are totally screened in the spectrum of $S3$ by the contribution from free carriers. Broad mid-ir absorption is not apparent to the untrained eye in the reflectance data.

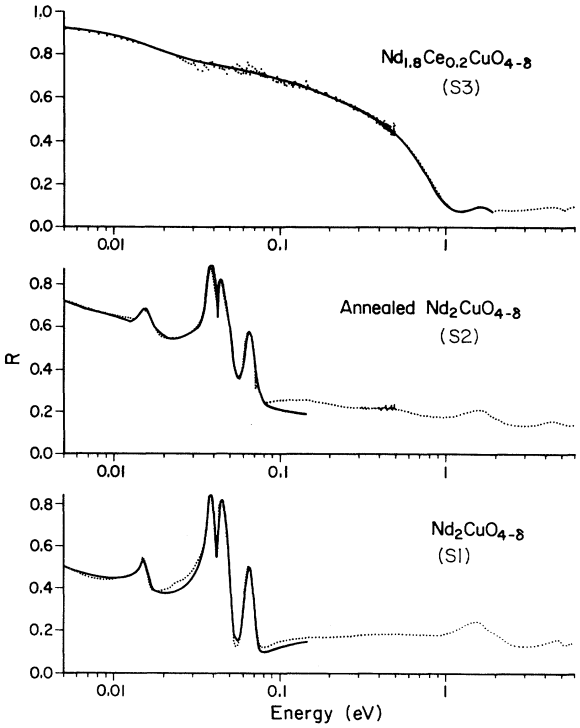

FIG. 1. Room-temperature a-b-plane reflectance R vs energy (eV) for $Nd_{2-x}Ce_xCuO_{4-\delta}$ crystals. Bottom panel ($S1$): as-grown $Nd_2CuO_{4-\delta}$ crystal; middle panel ($S2$): crystals $S1$ after a 900 °C anneal in He for 19 h, top panel ($S3$): as-grown $Nd_{1.8}Ce_{0.2}CuO_{4-\delta}$. The solid and dotted lines represent calculated and experimental results, respectively.

However, the mid-ir bands in $S1$, $S2$, and $S3$ can be seen clearly in the optical conductivity (σ_1) obtained from a Kramers-Kronig (KK) transformation of the reflectance data as discussed below.

IV. DISCUSSION

A KK analysis was carried out on the reflectance spectra of Fig. 1 to obtain the real and imaginary parts of the dielectric function $\epsilon=\epsilon_1+i\epsilon_2$. In the far-infrared region, the reflectivity data were extended either as a Drude metal (metallic sample) or a constant (nonmetallic samples). Tajima *et al.*[18] found that the reflectance spectrum of the La cuprates above 7 eV is not sensitive to doping. With this result in mind, we used the data of Tajima *et al.* for Nd_2CuO_4 as the high-energy-data extension ($6<\omega<40$ eV) for all three Nd-cuprate spectra. Finally, $R\sim a/(1+a\omega^4)$ was used as the extension for $\omega>40$ eV, where a is a constant, consistent with the usual high-energy free-electron response.

A. Phonons

The near-normal-incidence reflectance R is related to the dielectric function $\epsilon(\omega)$ by

$$R=\left|\frac{1-\sqrt{\epsilon}}{1+\sqrt{\epsilon}}\right|^2. \quad (1)$$

To determine the TO-phonon parameters from the reflectance data of undoped Nd_2CuO_4, we write $\epsilon(\omega)$ as

$$\epsilon(\omega)=\epsilon_\infty-\frac{\omega_p^2}{\omega(\omega+i\gamma_p)}+\sum_{j=1}^{n}\frac{\omega_{pi}^2}{\omega_j^2-\omega^2-i\omega\gamma_j}\ , \quad (2)$$

where ϵ_∞ is the core dielectric constant used to approximate the higher-frequency electronic polarizability. The second term is a free-carrier (Drude) term, where ω_p is the plasma frequency and $\gamma_p=1/\tau$ is the inverse carrier lifetime. The third term is a sum of Lorentz oscillators used to describe the respective ir-active, zone-center TO phonons, where ω_{pj}, ω_j, and γ_j are the strength, frequency, and damping for the jth mode, respectively.

In Fig. 1 the solid curves in the lower two panels ($S1$ and $S2$) represent the best fit to the R data using Eq. (2); the corresponding values for the TO-mode parameters appear in Table II. More generally, the TO- and LO-mode frequencies ω_{Tj} and ω_{Lj} are defined, respectively, as the poles and zeros of the dielectric function $\epsilon(\omega)$. Strictly speaking, when damping is involved, ω_{Tj} and ω_{Lj} are complex, and the imaginary part of the frequency stems from the mode damping. It is a matter of practical convenience to obtain the "real" TO- and LO-mode frequencies Ω_{Tj} and Ω_{Lj}, which correspond, approximately, to the maxima and the minima, respectively, of the modulus of the dielectric function, i.e., $|\epsilon|=(\epsilon_1^2+\epsilon_2^2)^{1/2}$.[19] In Figs. 2(a) and 2(b) we show various functions of $\epsilon(\omega)$ used to identify the LO- and TO-phonon parameters. The peaks in ϵ_2 or $|\epsilon|$ were used to obtain the TO-mode frequencies, whereas the peaks in $\mathrm{Im}(-1/\epsilon)$ and $(1/|\epsilon|)$ were used to obtain values for Ω_{Lj}. Finally, the TO-mode damping can be obtained either by fitting R or ϵ_2 with Eq. (2). All the phonon parameters are collected in Table II, where it can be seen that the changes in the TO-mode frequencies induced by the He anneal of the undoped material are negligible, typically less than 2 cm^{-1}, although other significant changes in the optical spectrum have occurred. On the other hand, the LO-mode frequencies are found to exhibit a larger change, $\sim$5–20 cm^{-1}, which may be significant, since these modes couple most strongly to free carriers created in the annealing process. The most significant change in the spectrum which is induced by the He anneal is in the free-carrier plasma frequency ω_p, where we find $\omega_p(S2)=3.1\omega_p(S1)$. It is most reasonable to assume that the increase in ω_p is due to an increase in the n-type carrier density ($\omega_p^2\sim n/m^*$, where n is the carrier density and m^* is the effective mass of the carrier).

$Nd_2CuO_{4-\delta}$ has been observed to have a tetragonal structure at room temperature with the space group $I4/mmm$.[18] Group theory predicts seven allowed ($q=0$) ir-active phonons: four polarized in the a-b plane (E_u modes) and three polarized along the c axis (A_u modes). This structure is similar to the tetragonal phase of La_2CuO_4 (Refs. 20–22) (A_u modes). This structure is similar to the tetragonal phase of La_2CuO_4,[22–24] the only difference between the two structures being that the out-of-plane oxygens are located on the faces at $(\frac{1}{2},0,\frac{1}{4})$ and equivalent positions in $Nd_2CuO_{4-\delta}$, whereas in La_2CuO_4 they lie directly above and below the copper atoms along the c axis at $(0,0,\pm v)$. We have calculated the zone-center ir-active phonon frequencies of $Nd_2CuO_{4-\delta}$ by means of the simple shell model used previously for La_2CuO_4.[4] The Nd atoms are located at the same (fractional) positions along the c axis as the La atoms in La_2CuO_4. The lattice constants $a=3.95$ Å and $c=12.07$ Å are taken from Ref. 23. The potential parameters in the current model are the same as we used in model 2 of

TABLE II. Phonon frequencies, phonon linewidths, and Drude parameters for $Nd_2CuO_{4-\delta}$ (all frequencies are in cm^{-1}).

Phonon mode	Parameter	This work Measured $S1$	This work Measured $S2$	This work Calculated	Crawford *et al.* (Ref. 23)[a] (expt.)	Degiorgi, Rusiecki, and Wachter (Ref. 13)[b] (expt.)	Wang *et al.* (Ref. 14)[c] (expt.)
E_{u1}	Ω_{T1}	121	121	137	129	121	139
	Ω_{L1}	138	153	139			
	γ_{T1}	16	20				
E_{u2}	Ω_{T2}	301	298	301	300	320	320
	Ω_{L2}	335	331	311			
	γ_{T2}	8	11				
E_{u3}	Ω_{T3}	347	347	340	350		594
	Ω_{L3}	426	436	504			
	γ_{T3}	12	8				
E_{u4}	Ω_{T4}	507	505	542	509	524	670
	Ω_{L4}	608	629	546			
	γ_{T4}	44	40				
ϵ_∞		7	7				
ω_p (cm^{-1})		1291	4033				
$\omega_p\tau$		0.64	0.91				

[a] $Nd_2CuO_{4-\delta}$ single crystal.
[b] Polycrystalline $Nd_{1.85}Ce_{0.15}CuO_{4-\delta}$ thin film.
[c] $Nd_{1.85}Ce_{0.15}CuO_{4-\delta}$ ceramic sample.

Ref. 18 for La_2CuO_4, except for a 5% increase in the Cu-O(1) Born-Mayer potential to remove negative eigenvalue along X-P-G_3. In Fig. 3 the displacements and symmetry of the four a-b-plane E_u modes allowed by group theory are illustrated using the eigenvectors calculated from the above shell model. The calculated TO E_{u2} frequency almost exactly matches the data; the other calculated TO frequencies differ by $\sim$10–35 cm^{-1} from the measured values (Table II). Considering that the only changes in our model calculation developed for La_2CuO_4 are the changes in structure and substitution of the Nd mass for the La mass, the agreement between experiment and theory for the TO modes is quite good. However, for the LO-mode frequencies that are more difficult to obtain optically, the agreement is substantially worse.

For comparison to the present results, we also list in Table II the TO-mode frequencies obtained by Crawford *et al.*,[23] Degiorgi, Rusiecki, and Wachter,[13] and Wang *et al.*[14] from other optical experiments. Crawford *et al.* also measured an undoped $Nd_2CuO_{4+\delta}$ single crystal, and their TO-mode results are in good agreement with ours. Degiorgi, Rusiecki, and Wachter's E_{u1} frequency on

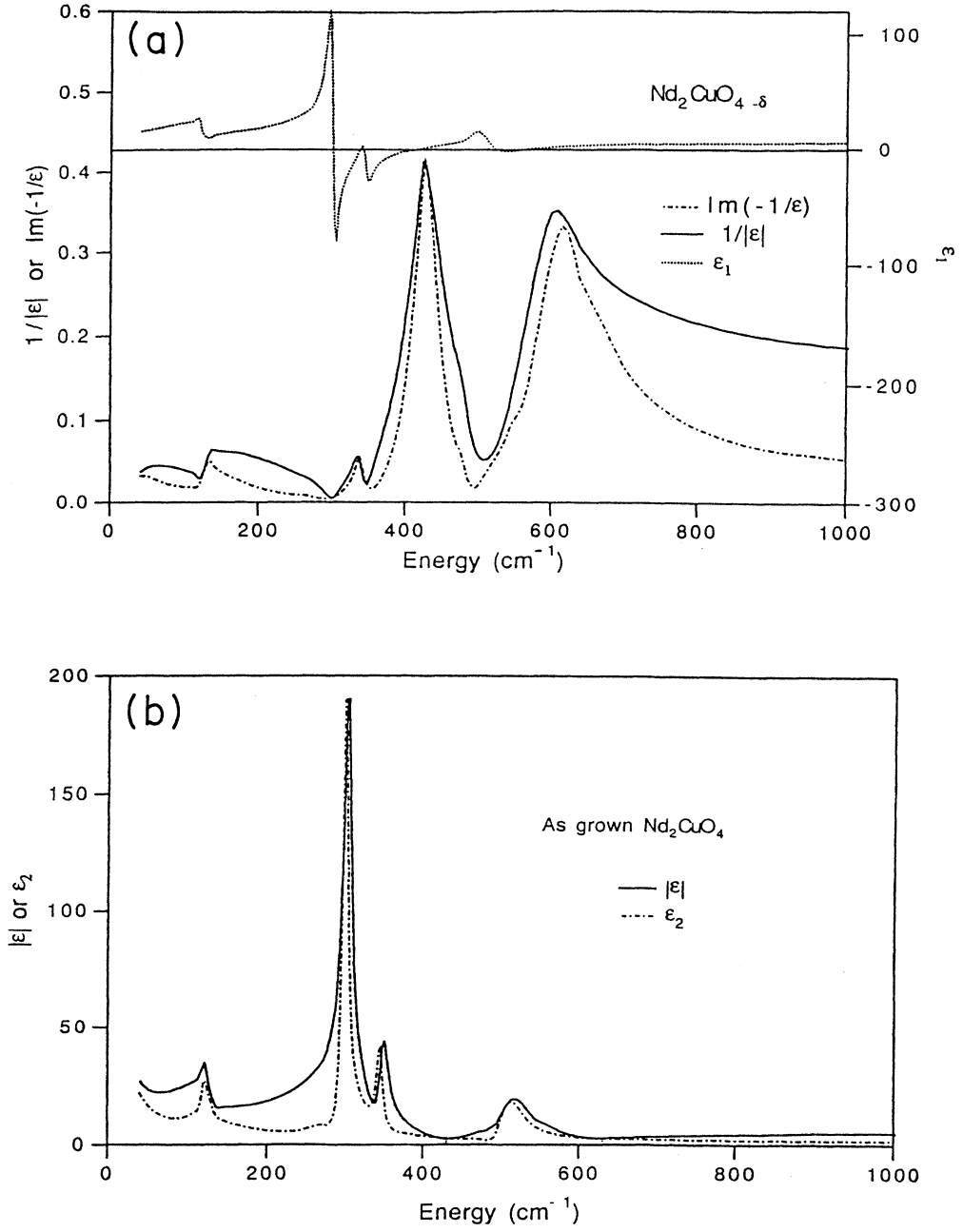

FIG. 2. (a) $1/|\epsilon|$, $\mathrm{Im}(-1/\epsilon)$, and ϵ_1 vs energy for Nd_2CuO_4 ($S1$, E⊥c). (b) $|\epsilon|$ and ϵ_2 vs energy for Nd_2CuO_4 ($S1$, E⊥c).

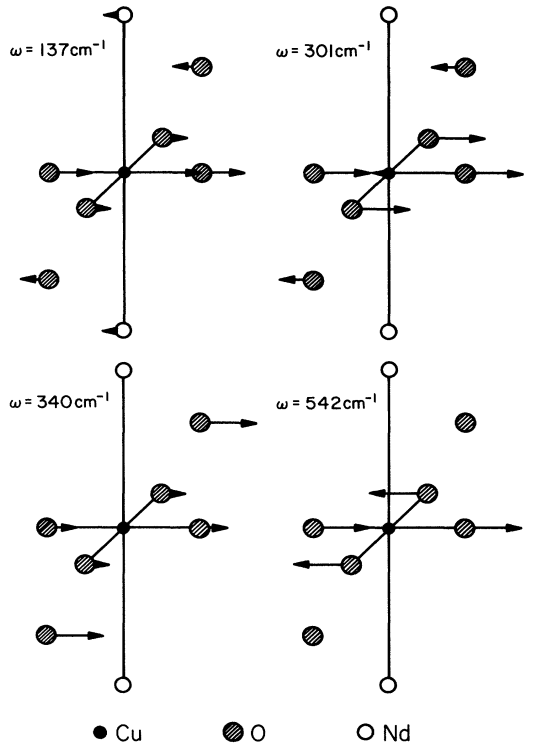

FIG. 3. Calculated zone-center displacements (E_u) for Nd_2CuO_4.

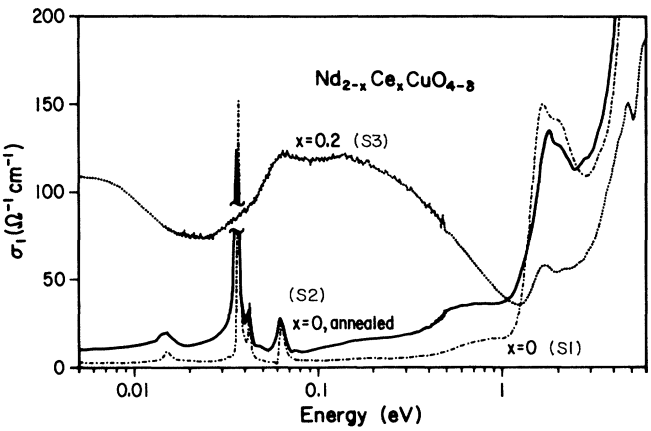

FIG. 4. Optical conductivity $\sigma_1(\omega)$ for $Nd_{2-x}Ce_xCuO_{4-\delta}$ crystal: The solid line is for as-grown $Nd_2CuO_{4-\delta}$ ($S1$), the dot-dashed line is for post-annealed $Nd_2CuO_{4-\delta}$ ($S2$), and the dotted line is for $Nd_{1.8}Ce_{0.2}CuO_{4-\delta}$ ($S3$).

polycrystalline $Nd_{1.85}Ce_{0.15}CuO_{4-\delta}$ thin films is identical with ours, their E_{u2} and E_{u4} values are ~ 20 cm^{-1} higher than the present results, and they did not detect the E_{u3} mode in their spectrum. Two TO frequencies obtained by Wang *et al.*[14] are quite different from the present results. This discrepancy may be attributed to the ceramic samples used in their study. As is well known from optical experiments on other high-T_c materials, it is difficult to extract quantitative information from polycrystalline samples.

B. Mid-ir absorption band

In Fig. 4 we plot the KK results for σ_1 on a logarithmic frequency scale, $\sigma(\omega)=i(\omega/4\pi)[\epsilon(\omega)-1]=\sigma_1+i\sigma_2$, where the real part of the optical conductivity σ_1 is identified with optical absorption. The sharp peaks below ~ 0.1 eV in the conductivity data for samples $S1$ and $S2$ are associated with the in-plane TO modes. Because of screening from the free carriers, a similar phonon structure cannot be detected in the Ce-doped sample ($S3$). Broad absorption is observed in all three σ_1 curves from the far-ir to 1 eV, which, consistent with the terminology in the literature,[2] we term the "mid-ir" band. The strength of the band is correlated with doping, i.e., via oxygen defects ($\delta \neq 0$) or Ce substitution ($x \neq 0$). Sample $S1$ exhibits a very weak mid-ir band. However, after a post-anneal in He at 900 °C for 19 h (i.e., a reducing environment), the strength of this band grows noticeably as shown in the spectrum for $S2$. Ce doping at 10% ($S3$), enhances even further the strength of the mid-ir absorption, and the oscillator strength shifts to lower frequency. Similar to a report by Hirochi *et al.*,[15] it is evident from Fig. 4 that the growth of the mid-ir absorption proceeds at the expense of the oscillator strength of the peak at 1.6 eV. Hirochi *et al.*[15] identified the mid-ir absorption in the 2.5–1.0-μm region of their spectra of Ce-doped $NdCuO_4$ films with free-carrier absorption, fitting their data to a Drude-like, free-carrier term. However, a Drude-like free-carrier conductivity would continue to rise with decreasing ω in the far-ir, saturating at zero frequency to $\sigma_1(0)=\omega_p^2\tau/4\pi$, where τ is the free-carrier relaxation time. Clearly, this type of far-ir behavior is not observed for $S3$ ($x=0.2$), as a noticeable notch appears in the data at ~ 20 meV (see Fig. 4). This notch is not an artifact of the KK analysis, as we discuss below.

In Fig. 5 we show how the optical conductivity in the far-ir is affected by the data extension below 40 cm^{-1} (5 meV). The $\sigma_1(\omega)$ results for $S3$ are plotted on a linear frequency scale for the following far-ir data extensions: (a) $R=0$, (b) $R=1-K_1\omega$, (c) $R=K_2$, and (d) $R=1-(K_3\omega)^{1/2}$, where the K_j are constants. The extension (d) is consistent with the Drude model. As can be seen in the figure, the notch in the σ_1 data is present in every case, and is therefore not an artifact of the far-ir extension. We next discuss models with which we have attempted to fit the optical data for the Ce-doped sample, i.e., the marginal-Fermi-liquid model[25] (MFL) and the modified Drude-Lorenz model[3] (MDL).

Varma, Littlewood, and Schmitt-Rink proposed the phenomenological, marginal-Fermi-liquid model to explain universal anomalies in the normal state of cuprate superconductors. In their model the mid-ir band is associated with excitations of a marginal Fermi liquid. The conductivity σ_1 derived from their MFL model can be written, for $\omega < T$,

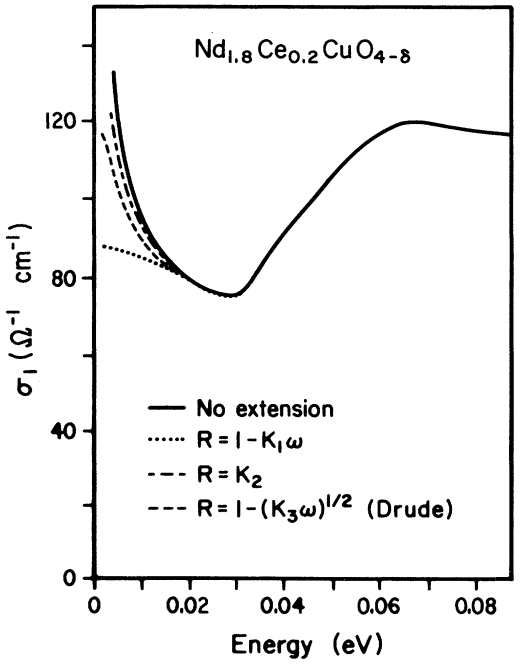

FIG. 5. Effect of various low-energy R data extensions on the low-frequency optical conductivity of $Nd_{1.8}Ce_{0.2}CuO_{4-\delta}$ ($S3$). The data have been smoothed by fitting to a polynomial; the raw data is shown in Fig. 6. Note that the notch in the conductivity is not affected by the form of the far-ir data extension.

$$\sigma_1=\left[\frac{\alpha}{T}\right]C(\omega)+\frac{\omega_p^2}{4\pi}\left[\frac{A}{1+[A\omega^2-(2\omega^2/\pi T)\ln(T/\omega_c)]^2}\right], \quad (3a)$$

and, for $\omega > T$,

$$\sigma_1=\alpha\omega C(\omega)+\frac{\omega_p^2}{4\pi}\left[\frac{A}{1+[AT-(2/\pi)\ln(\omega/\omega_c)]^2}\right], \quad (3b)$$

where α and ω_c are constants, $A=1/(g^2N^2\pi T/2)$, N is the unrenormalized one-particle density of states, T is temperature, and g is a coupling constant. The form of the spectral cutoff factor $C(\omega)=[1+(\omega/\omega_c)^2]^{-1}$ is arbitrary, yet it directly affects the shape of the high-energy tail of the mid-ir band. ω_p is the plasma frequency of the strongly interacting free carriers in the MFL. The first term in Eq. (3) gives rise to the mid-ir band, and the second term is the renormalized free-carrier conductivity.

For single-crystal $La_{1.8}Sr_{0.2}NiO_4$,[3] we also found a broad mid-ir absorption band similar to that of $S3$ in Fig. 4, but with a band maximum at higher energy, i.e., ~ 0.6 eV. The MDL, rather than the MFL model, was found to best fit the $La_{1.8}Sr_{0.2}NiO_4$ data. However, it can be argued, of course, that La_2NiO_4 is not a bona fide member

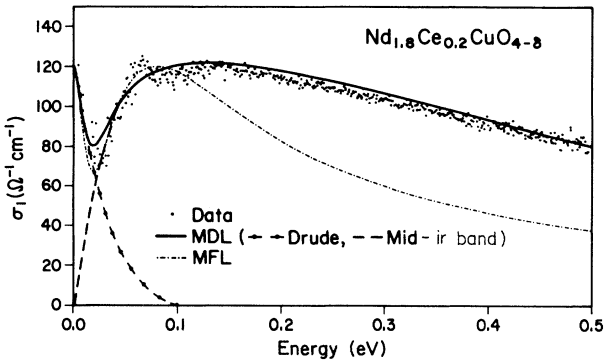

FIG. 6. Conductivity data for $Nd_{1.8}Ce_{0.2}CuO_{4-\delta}$ ($S3$) in the energy range 0–0.5 eV. The dotted, dot-dashed, and solid lines refer, respectively, to the data, the MFL model, and the MDL model. See the text for the details of the model calculation.

of the high-T_c oxide superconducting family, although diamagnetism equivalent to a 1% Meissner effect has been observed.[16] The conductivity $\sigma_1(\omega)$ for the MDL model is calculated according to[2]

$$\sigma_1=\frac{\omega_p^2\tau/4\pi}{1+\omega^2\tau^2}+\frac{\omega^2\omega_e^2\gamma_e/4\pi}{(\omega^2-\omega_e^2)^2+\gamma_e^2\omega^2}. \quad (4)$$

The first term is the free-carrier contribution in the Drude approximation, and the second term is a Lorentz oscillator identified with the mid-ir band.

In Fig. 6 we show the $T=300$ K optical conductivity data of $Nd_{1.8}Ce_{0.2}CuO_{4-\delta}$ single crystals on a linear frequency scale up to 0.5 eV. The results of calculations according to the MFL (dot-dashed line) and MDL (solid line) model are shown for comparison, and the values for the fitting parameters can be found in Table III. The dashed lines in the figure represent the individual contributions in the MDL model from the free carrier and mid-ir absorption band. It should be noted that the frequency dependence of the high-energy tail of the mid-ir band is similar to that of Drude free-carrier conductivity, i.e., $\sigma_1\sim\omega^{-2}$, and a fit of a Drude model to this tail produces a value for the plasma frequency of $S3$ of $\omega_p\sim 2$ eV, much higher than the values we obtain from fitting the MDL model ($\omega_p=0.28$ eV) or the MFL model ($\omega_p=0.13$ eV) to the data (see Table IV). Hirochi *et al.*,[15] in film studies on Ce-doped Nd_2CuO_4, obtained values $\omega_p\sim 1$ eV from a Drude fit to the high-energy tail of the mid-ir band. Since the carrier effective mass $m^*\sim\omega_p^{-2}$, a Drude fit to the high-energy tail of the mid-ir band, rather than to the far-ir data, results in a factor of 10–20 lower effective mass. Thus literature values for

TABLE III. Marginal Fermi liquid (MFL) model parameters for $Nd_{1.8}Ce_{0.2}CuO_{4-\delta}$.

ω_p (eV)	α	$gN(0)$	ω_c (eV)
0.13	8	5.8	0.2

TABLE IV. Drude-Lorentz parameters for $Nd_{1.8}Ce_{0.2}CuO_{4-\delta}$.

ϵ_∞	ω_p (eV)	$\omega_p\tau$	Ω_e (eV)	ω_e (eV)	γ_e (eV)
3.5	0.28	20	1.91	0.136	0.65
			0.91	1.80	0.62

the effective mass determined optically should be viewed with caution.

It should be noted that the MDL and MFL models are both capable of generating a notch in σ_1 at $\sim$24 meV, in good agreement with the $S3$ data. However, the MFL model cannot fit the high-energy tail of the mid-ir band: This region is dominated by the arbitrary cutoff factor $C(\omega)$ in Eq. (3). On the basis of the fits (Fig. 6) below 0.1 eV, it is really not possible to say where the MFL or MDL model fits the data best. A good optical test of the MFL model would come from a temperature study of the far-ir notch in the σ_1 data. According to Eq. (3) of the MFL model, this notch frequency ω_n should be approximately equal to kT. The present experimental value $\omega_n=0.024$ eV is indeed quite close to $kT=0.026$ eV.

C. Conductivity and the carrier density

By extrapolating the far-ir $\sigma_1(\omega)$ to $\omega=0$, we may determine a value for the dc conductivity of the three samples. For as-grown $Nd_2CuO_{4-\delta}$, we obtain an optical value for the dc conductivity $\sigma_1(0)\sim 2.2\ (\Omega\,\mathrm{cm})^{-1}$. After helium annealing, $\sigma_1(0)$ increased to $9.7\ (\Omega\,\mathrm{cm})^{-1}$. $\sigma_1(0)$ for the cerium-doped sample ($S3$) is much higher, i.e., $\sigma_1(0)\sim 120\ (\Omega\,\mathrm{cm})^{-1}$. These results are in reasonable agreement with the transport values of Tokura, Takagi, and Uchida,[1] who reported for ceramic $Nd_2CuO_{4-\delta}$ $\sigma_{dc}\sim 5\ (\Omega\,\mathrm{cm})^{-1}$. They also reported that σ_{dc} increases two orders of magnitude after annealing in air, followed by a rapid quench. They indicate this process produces an oxygen deficiency $\delta\sim 0.04$. Uji, Aoki, and Matsumoto[5] reported $\sigma_{dc}=0.6$ and $\sim 500\ (\Omega\,\mathrm{cm})^{-1}$ for $x=0$ and 0.2, respectively; neither sample was reduced. All these conductivity data (and supporting Hall-effect data[1]) indicate that both oxygen deficiences and/or cerium doping introduce mobile electrons into the Nd cuprates.

The room-temperature effective mass m^* of the Ce-doped sample can be estimated from our results as follows. On the basis of x-ray measurements by Huang *et al.*,[20] the average valence of Nd and Ce in $Nd_{1.8}Ce_{0.2}CuO_{4-\delta}$ is 3 and 3.84, respectively, and so every Ce atom substituted for Nd will contribute 0.84 electrons. Assuming that all charge carriers are introduced via cerium doping, the carrier density n_3 obtained is $n=0.2\times 0.84$ per formula unit (f.u.)$=3.57\times 10^{21}$ cm^{-3}, using 2 f.u. per unit cell of volume $V=94.1$ Å^3.[1] Using the relation $\omega_p^2=4\pi ne^2/m^*$, we find that the effective mass m^* is surprisingly large: $m^*=62m_0$, where m_0 is the free-electron mass. The above result can be compared to the value $m^*\sim 34m_0$ obtained similarly for p-type $La_{1.8}Sr_{0.2}NiO_4$ single crystals.[3] The large values obtained for the mass indicate that the Drude model is probably not an appropriate description for the itinerant electrons in these materials. The value of the mass suggests that polaron formation may likely occur. However, we emphasize again that value of the effective mass determined optically should be regarded with caution.

D. Higher-energy interband structures

A sharp increase in the optical conductivity σ_1 (dot-dashed line, Fig. 4) is observed at 1.3 eV in the as-grown $Nd_2CuO_{4-\delta}$ crystal ($S1$). We identify this increase with the charge-transfer (CT) energy gap at 1.3 eV. The excitations across this gap occur between O($2p$) states (valence band) and higher-energy Cu($3d$) states or the upper Hubbard band (conduction band).[15] Tajima *et al.* previously observed this broad absorption edge in $Nd_2CuO_{4-\delta}$ at 1.5 eV.[18] As we have discussed above, annealing at 900 °C in He reduces the strength of these CT transitions between 1 and 3 eV (solid line in Fig. 4). Furthermore, when cerium ions are introduced ($x=0.2$, dotted line in Fig. 4), the strength of these CT transitions is even further reduced.

The oscillator strength $f(E)$ in the energy interval from zero to E is given by[26]

$$f(E)=N_{\mathrm{eff}}\left[\frac{m}{m^*}\right]=\frac{2m}{\pi e^2 N_{\mathrm{Cu}}}\int_0^E \sigma_1(\omega)d\omega\ , \tag{5}$$

where m and e are the mass and charge of the free electron. N_{eff} is the effective density of electrons, with effective mass m^* participating in the absorption at energies less than E, and is normalized to the density of Cu atoms N_{Cu}. The calculated oscillator strength $f(E)$ for $S1$, $S2$, and $S3$ are plotted against energy E in Fig. 7. It is clear that all oscillator strengths reach about the same value at $E=2.3$ eV, the same energy where all three conductivity curves show a local minimum (see Fig. 4). Thus

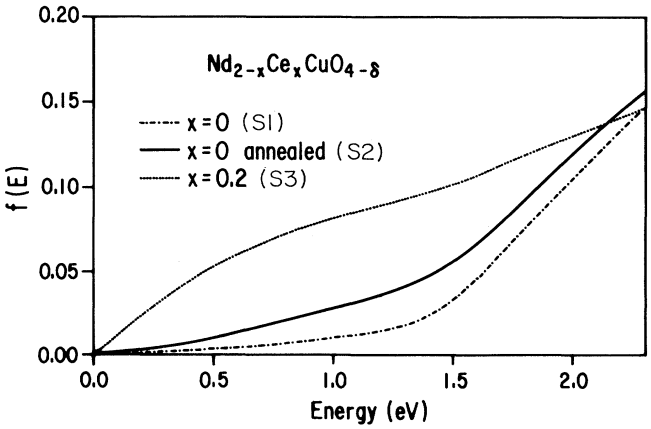

FIG. 7. Oscillator strength as a function of energy for the three $Nd_{2-x}Ce_xCuO_{4-\delta}$ samples.

there appears to be a simple downshift of oscillator strength from 1–2.3-eV CT excitations to the mid-ir band. The observed correlation between the oscillator strength in the mid-ir band and CT excitation is interesting, particularly in view of the previous noted correlation of T_c and the strength of the mid-ir band.

ACKNOWLEDGMENTS

This work was sponsored by the University of Kentucky Research Foundation and the Electrical Power Research Institute. We are grateful to Professor J. M. Honig, Dr. J. Spalek, and Dr. P. B. Littlewood for helpful discussions.

*Permanent address: Université de Nancy, Faculté des Sciences, Laboratoire de Chimie Minérale Appliquée, B.P. 239-54506, Vandoeuvre-les-Nancy CEDEX, France.

[1]Y. Tokura, H. Takagi, and S. Uchida, Nature **337**, 345 (1989).

[2]T. Timusk and D. B. Tanner, in *Physical Properties of High Temperature Superconductors,* edited by D. M. Ginsberg (World Scientific, Singapore, 1989).

[3]X. X. Bi, P. C. Eklund, E. McRae, J. G. Zhang, P. Metcalf, J. Spalek, and J. M. Honig, Phys. Rev. B **42**, 4756 (1990).

[4]M. Mostoller, J. G. Zhang, and P. C. Eklund, Phys. Rev. B **41**, 6488 (1990).

[5]S. Uji, H. Aoki, and T. Matsumoto, Jpn. J. Appl. Phys. **28**, L563 (1989).

[6]P. H. Hor, Y. Y. Xue, Y. Y. Sun, Y. C. Tao, Z. J. Huang, W. Rabalais, and C. W. Chu, Physica C **159**, 629 (1989).

[7]T. Ekino and J. Akimitsu, Phys. Rev. B **40**, 7364 (1989).

[8]M. Abe, K. Kumagai, S. Awaji, and T. Fujita, Physics C **160**, 8 (1990).

[9]A. Grassmann, J. Strobel, M. Klauda and J. Schlotterer, Europhys. Lett. **9**, 827 (1989).

[10]J. L. Peng, R. N. Shelton, and H. B. Radousky, Phys. Rev. B **41**, 187 (1990).

[11]S. I. Hatta, S. Hayashi, H. Adachi, and K. Wasa, Jpn. J. Appl. Phys. **28**, L1201 (1989).

[12]G. Lian, J. Chen, M. Croft, K. V. Ramanujachary, M. Greenblatt, and M. Hegde, Phys. Rev. B **40**, 2646 (1989).

[13]L. Degiorgi, S. Rusiecki, and P. Wachter, Physica C **161**, 239 (1989).

[14]S. H. Wang, Q. Song, B. P. Clayman, J. L. Peng, L. Zhang, and R. N. Shelton, Phys. Rev. Lett. **64**, 1067 (1990).

[15]K. Hirochi, S. Hayashi, H. Adachi, T. Mitsuyu, T. Hirao, K. Setsune, and K. Wasa, Physica C **160**, 273 (1989).

[16]J. M. Honig (private communication).

[17]J. G. Zhang, Ph.D. dissertation, University of Kentucky, 1990 (unpublished).

[18]S. Tajima, H. Ishii, T. Nakahashi, T. Takagi, S. Uchida, M. Seki, S. Suga, Y. Hidaka, M. Suzuki, T. Murakami, K. Oka, and H. Unoki, J. Opt. Soc. Am. B **6**, 475 (1989).

[19]Both Ω_{Tj} and Ω_{Lj} can be easily identified from the plot of $|\epsilon|$. It can be shown that in the approximation $\gamma_j = \gamma_{Tj} \ll \omega_j$ and ω_{pj}, Ω_{Tj} will reduce to ω_j and Ω_{Lj} will correspond to the peak positions of $\mathrm{Im}(-1/\epsilon)$. See Ref. 17 for details.

[20]T. C. Huang, E. Moran, A. I. Nazzal, and J. B. Torrance, Physica C **158**, 148 (1989).

[21]A. Khurana, Phys. Today **42**(4) (1989).

[22]H. Takagi, S. Uchida, and Y. Tokura, Phys. Rev. Lett. **62**, 1197 (1989).

[23]M. K. Crawford, G. Burns, G. V. Chandrashekhar, F. H. Dacol, W. E. Farneth, E. M. McCarron III, and R. J. Smalley, Bull. Am. Phys. Soc. **35**, 783 (1990).

[24]J. Orenstein, G. Thomas, D. H. Rapkine, C. G. Bethea, B. F. Levine, B. Batlogg, R. J. Cava, D. W. Johnson, Jr., and E. A. Rietman, Phys. Rev. B **36**, 8892 (1987).

[25]C. M. Varma, P. B. Littlewood, and S. Schmitt-Rink, Phys. Rev. Lett. **63**, 1996 (1989).

[26]F. Wooten, *Optical Properties of Solids* (Academic, New York, 1972).